Transmission Line Matrix Model for Detection of Local Changes in Permeability Using a Microwave Technique

Razvan Ciocan, *Member, IEEE,* and Nathan Ida, *Member, IEEE*

Abstract—A three-dimensional transmission-line matrix model was developed to simulate the microwave detection of local changes in permeability. The technique can be used to map local nonuniformities in magnetization. Numerical modeling was carried out for frequencies that are commonly used in microwave nondestructive testing (0.8–1 GHz). A comparison between experimental and numerically generated curves is provided. This comparison validated the proposed numerical model.

Index Terms—Microwaves, nondestructive testing and evaluation, transmission-line matrix (TLM) method.

I. INTRODUCTION

THE FIRST microwave probe capable of measuring the spatial variation of magnetic properties was proposed in 1962 [1]. The possibility to perform microwave measurements on thin ferromagnetic layers in a magnetic field was demonstrated recently [2], [3]. A fully theoretical model for these techniques in various geometries is almost impossible to obtain. For this reason, a numerical model that is unconditionally stable and capable of modeling different geometries is very attractive and very useful for future development of these investigation techniques.

The transmission-line matrix (TLM) is a timte-domain numerical technique that is well suited for modeling of complex geometries [4]. The method is a direct numerical implementation of the Huygens principle. The wave front at each iteration for a certain mesh node is a result of the waveforms generated at neighboring nodes in the previous iteration. The TLM is a physical discretization approach and does not require the solution of the differential equation in the whole space being modeled. The solution of the differential equation is implemented only for the smallest entity (called node) that can be modeled using TLM method in the scattering matrix formulation. The coefficients of this matrix are obtained in such a way that charge and flux conservation laws are obeyed for the node. This method is recognized for its unconditional convergence that is achieved for dimensions of nodes less than one tenth of a wavelength [5]. Numerical results were obtained using the symmetrical condensed node (SCN) [6]. A new numerical model based on the TLM method for microwave detection of local variation in perme-
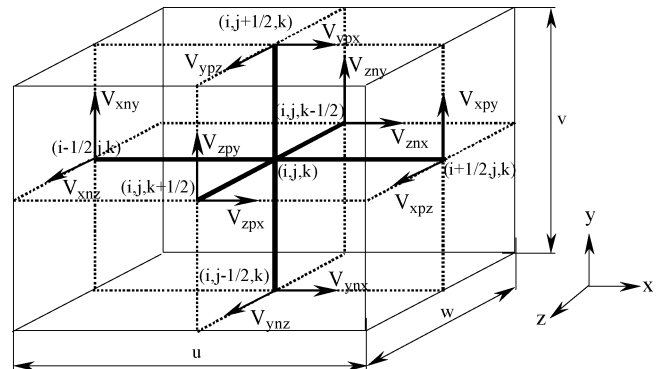
Fig. 1. Symmetrical condensed node for a parallelepipedic region of space with dimensions u, v, and w.

ability is proposed in this paper. Section II presents an algorithm description. Section III contains a discussion of the obtained results, and Section IV presents the conclusion of this work.

II. ALGORITHM DESCRIPTION

A. TLM and Finite-Difference Timte-Domain Formulations

The TLM equations for the field components are written as a function of the voltages on the node edges. The three-index notation used in this paper (Fig. 1) is related to the position of the ports and to the direction of link lines [7]. For example, V_{xpy} is the voltage pulse on a link line parallel to the x axis ("x" index), on the positive side ("p" index), and polarized in the y direction ("y" index).

A full derivation of field quantities obtained in an FDTD formulation is given in [8]. The field derivation is based on the rationale of Jin and Vahlidieeck, but here it was developed in the three-index notation [9].

Following this derivation, it is shown that the field quantities in the middle of the cubic node (with a side of Δl) are written as a function of incident voltages on node faces

$$E_x = -\frac{1}{2\Delta l}\left(V_{ynx}^i + V_{ypx}^i + V_{zpx}^i + V_{znx}^i\right) \tag{1}$$

$$E_y = -\frac{1}{2\Delta l}\left(V_{xny}^i + V_{xpy}^i + V_{zpy}^i + V_{zny}^i\right) \tag{2}$$

$$E_z = -\frac{1}{2\Delta l}\left(V_{xnz}^i + V_{xpz}^i + V_{ypz}^i + V_{ynz}^i\right) \tag{3}$$

$$H_x = \frac{V_{zny}^i - V_{ynz}^i + V_{ypx}^i - V_{zpy}^i}{2Z_o\Delta l} \tag{4}$$

$$H_y = \frac{V_{xnz} + V_{zpx} - V_{xpz} - V_{znx}}{2Z_o \Delta l} \tag{5}$$

$$H_z = \frac{V_{xpy} - V_{ypx} - V_{xyz} + V_{ynx}}{2Z_o \Delta l}. \tag{6}$$

To reveal the differences between the TLM algorithm based on symmetrical node and the three-dimensional finite-difference timte-domain (FDTD) Yee's scheme we start with the source-free Maxwell's equations for an isotropic medium in rectangular coordinates [10]

$$\varepsilon_0 \frac{\partial E_x}{\partial t} = \frac{\partial H_z}{\partial y} - \frac{\partial H_y}{\partial z} \tag{7}$$

$$\mu_0 \frac{\partial H_x}{\partial t} = \frac{\partial E_y}{\partial z} - \frac{\partial E_z}{\partial y}. \tag{8}$$

Equations (7) and (8) are written using Yee's scheme with central difference approximations as [10]

$$
\begin{aligned}
{}_n E_x &\left(i + \frac{1}{2}, j, k\right) - {}_{n-1} E_x \left(i + \frac{1}{2}, j, k\right) \\
&= s Z_0 \left({}_{n-\frac{1}{2}} H_x \left(i + \frac{1}{2}, j + \frac{1}{2}, k\right) \right. \\
&\qquad \left. - {}_{n-\frac{1}{2}} H_z \left(i + \frac{1}{2}, j - \frac{1}{2}, k\right) \right) \\
&\quad - s Z_0 \left({}_{n-\frac{1}{2}} H_y \left(i + \frac{1}{2}, j, k + \frac{1}{2}\right) \right. \\
&\qquad \left. + {}_{n-\frac{1}{2}} H_z \left(i + \frac{1}{2}, j, k - \frac{1}{2}\right) \right)
\end{aligned}
\tag{9}
$$

$$
\begin{aligned}
{}_{n+\frac{1}{2}} H_x &\left(i, j + \frac{1}{2}, k + \frac{1}{2}\right) - {}_{n-\frac{1}{2}} H_x \left(i, j + \frac{1}{2}, k + \frac{1}{2}\right) \\
&= s \frac{1}{Z_0} \left({}_n E_y \left(i, j + \frac{1}{2}, k + 1\right) - {}_n E_y \left(i, j + \frac{1}{2}, k\right) \right) \\
&\quad - s \frac{1}{Z_0} \left({}_n E_y \left(i, j + 1, k + \frac{1}{2}\right) \right. \\
&\qquad \left. - {}_n E_y \left(i, j, k + \frac{1}{2}\right) \right).
\end{aligned}
\tag{10}
$$

Equations (9) and (10) were written for a point (Fig. 1) located at (i, j, k) at instant n. The stability factor s was introduced in (9) and (10) and is defined as

$$s = c \frac{\Delta t}{\Delta l}. \tag{11}$$

For a cubic node, in free space, the stability factor is found to be [10]

$$\sqrt{3(\Delta l)^2} \geq c \Delta t \Rightarrow s \leq \frac{1}{\sqrt{3}}. \tag{12}$$

A similar value was determined from dispersion relation analysis [11]. This condition is automatically satisfied in TLM (SCN node) because the speed of propagation in a TLM based on the SCN node is [12]

$$c_{\max} = \frac{\Delta l}{\Delta t} = \frac{c}{\sqrt{2}}. \tag{13}$$

The main advantage of TLM (SCN node) over FDTD (Yee's scheme) consists in modeling discontinuities and sources. Field components for TLM are computed at the same location in time and in space while in FDTD—at alternate time steps and at half space increments. The left index of the fields in (9) and (10) specifies the time when the quantity is evaluated. In Yee's scheme the electric and magnetic field components are computed at alternate time steps and at half space increments. This is in contrast with the TLM algorithm based on the SCN, where all field components are computed at the same location in time and space, as shown in (1)–(6). This is the main difference between an FDTD and a TLM scheme based on the SCN node. The immediate benefit of having all field components at the same point consists in modeling space discontinuities. Furthermore, the stability criterion required by (12) for the FDTD scheme is automatically satisfied by any TLM scheme.

Comparison between TLM and FDTD in reported results obtained on the same structure and using the same mesh size shows a better accuracy for the TLM scheme [13], [14]. The price for this consists in increased computer memory resources as compared with FDTD: a TLM algorithm based on the SCN node needs 24 additions, 12 multiplications, and 12 variables to be stored per node [15]. The FDTD algorithm requires 24 additions, 12 multiplications, and 6 variables to be stored per node [16].

B. TLM Algorithm Implementation

The main steps of a TLM algorithm are initialization, scattering and connection. An additional step, called scanning, was added to these components. This step involves changing the position of excitation according to the experimental scanning pattern whereby the TLM algorithm is repeated for each new position. The time response for each position is saved in an output file for further processing. In the initialization step, a Gaussian modulated pulse is injected in the TLM mesh in the position of the microwave probe. The voltage injected is given by

$$V^i(x, y) = A e^{-(t-t_o)^2/2\sigma^2} \cos(2\pi f(t - t_o) + \varphi). \tag{14}$$

In (14), the following notations were used: A = amplitude; σ = standard deviation; t = time; t_o = delay; f = frequency; φ = phase. The pulse parameters have been modified to obtain the best fit with a reflected signal from a material with known permeability. In further experiments these parameters were kept the same. The scattering matrix was implemented according to the methodology proposed by Trenkic [17]. This method is based on an algorithm that explores the symmetry of the scattering matrix and decreases the number of operations needed. The voltages at all ports are obtained using the following equations:

$$V_{inj}^r = V_{\text{temp}} - V_{\text{dif}} \tag{15}$$

$$V_{ipj}^r = V_{\text{temp}}. \tag{16}$$

In (15) and (16), the following notations were used:

$$V_{\text{temp}} = \frac{1}{2}(V_{kni} + V_{kpi} + V_{\text{dif}}) \tag{17}$$

$$V_{\text{dif}} = V_{ipj} - V_{inj}. \tag{18}$$

The voltages are obtained considering all circular permutations of indexes (x, y, z) denoted in general form as (i, j, k). The parameter used to obtain the microwave image is the scattering parameter, S_{11}. This parameter cannot be obtained directly from
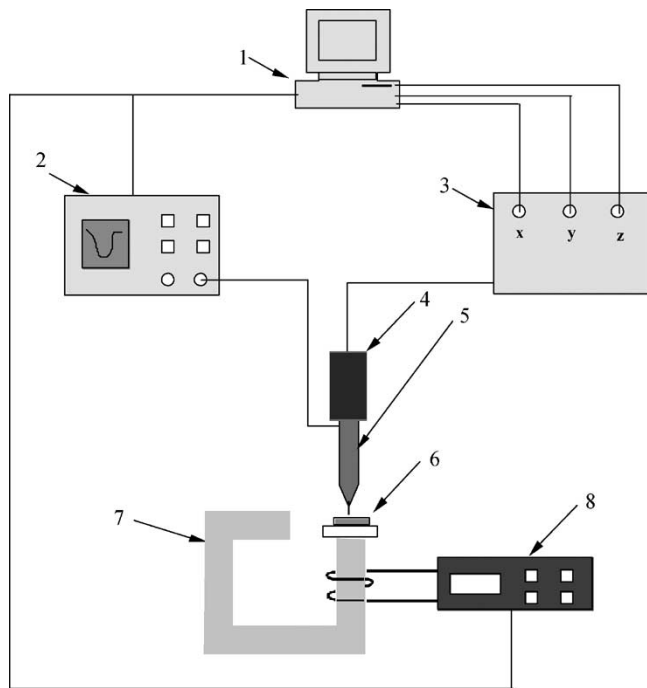
Fig. 2. Block diagram of the experimental setup. 1: computer; 2: network analyzer; 3: stepper motor controller; 4: port-probe assembly; 5: microwave probe; 6: sample; 7: electromagnet; 8: voltage source.

the TLM algorithm because the incident field cannot be separated. To solve this problem, two successive runs of the program are needed. The first run is performed with excitation without a reflecting object. This run will provide data for the reference port. A second run of the program will be performed considering boundary conditions for objects to be investigated. The S_{11} parameter is given by [18]

$$S_{11} = \frac{F_i - F_0}{F_i + F_0}. \tag{19}$$

In (19), F_0 and F_i are the frequency responses obtained for the same position of the excitation source without reflecting object and with reflector respectively.

III. RESULTS

An experimental setup (Fig. 2) was designed for this application [19]. In this setup, the magnetic sample (six in Fig. 2) was placed over an electromagnet (seven in Fig. 2) that was energized by a dc current from voltage source (eight in Fig. 2). The sample and the electromagnet assembly were located underneath the microwave probe (five in Fig. 2). The personal computer (1 in Fig. 2) controlled the movement of the microwave probe via a stepper motor controller (three in Fig. 2). The network analyzer (two in Fig. 2) and voltage source were controlled by computer via GPIB interface. The electromagnet used in the present work produced 250 G at 100 mA (16 V) and its B versus I characteristics were approximately linear in that range as determined with a Gauss meter.

The microwave probe was operated in reflection mode [20]. The probe position over the sample could be changed using various micrometers and stepping motors.
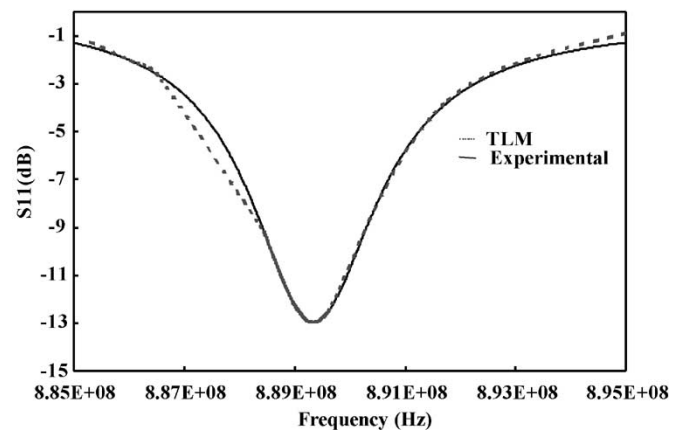
Fig. 3. Comparison between numerical (dashed line) and experimental frequency responses obtained in the absence of an external magnetic field.
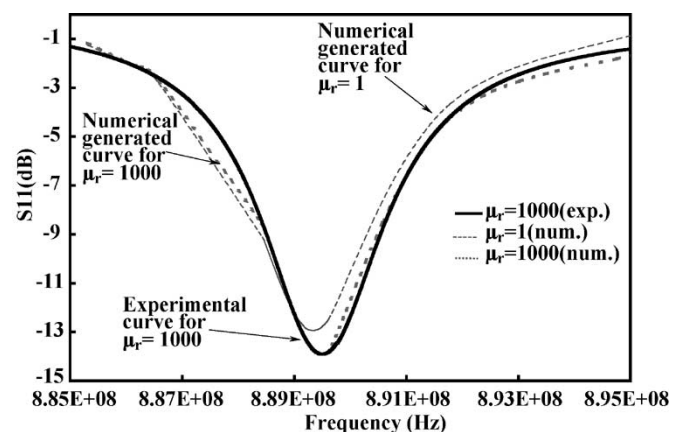
Fig. 4. Frequency responses obtained in absence and in presence of magnetic field.

TABLE I
COMPARISON BETWEEN NUMERICAL AND EXPERIMENTAL DATA

Type of data	μ_r	Frequency (MHz)	S_{11} (dB)
Numerical	1	889.32	-12.94
Numerical	1000	889.51	-13.91
Experimental	1	889.31	-12.93
Experimental	1000	889.49	-13.90

Fig. 3 shows a comparison between numerical and experimental resonance curves obtained for a CO-NETIC alloy sample in the absence of the external magnetic field. The values for relative permeability were obtained from product catalog (CO-NETIC & NETIC, Magnetic Shielding Alloys Obtained From Magnetic Shield Corp.). The graph shows good agreement between experimental and numerical data.

To obtain a similar resolution in frequency domain for experimentally and numerically generated curves ($\Delta f_{exp} = 10$ kHz) a zero padding procedure was applied to numerical data. The microwave probe detects the relative change in magnetic permeability by changing its frequency response as it is shown in Fig. 4. This change was 190 kHz and 1 dB for numerical data. Similar values were obtained for experimental data (Table I).

In order to prove that the system can detect a nonuniformity in magnetization, the values of the S_{11} parameter obtained at
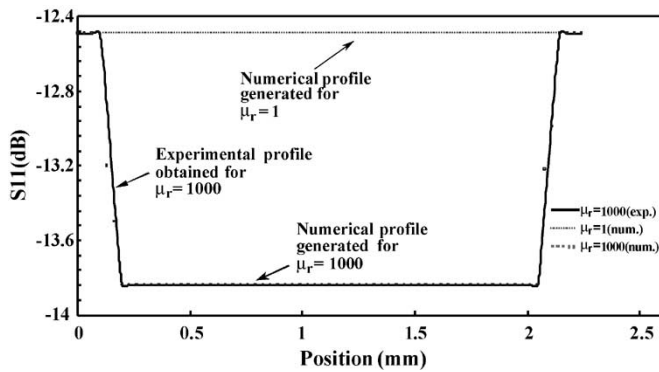
Fig. 5. Numerical and experimental profiles obtained at scanning over a 2-mm sample.

889.61 kHz, when the microwave probe was scanned over a 2-mm sample, were plotted in Fig. 5.

IV. CONCLUSION

A numerical model for scanning microwave microscopy was implemented for magnetic materials. The model is based on the TLM algorithm. The experimental results obtained by the authors validate the proposed numerical model. The scanning process was also implemented into the numerical model. This allows a better characterization of discontinuities in magnetic permeability detected using microwave techniques.

REFERENCES

[1] R. F. Soohoo, "A microwave magnetic microscope," *J. Appl. Phys.*, vol. 33, no. 3, pp. 1276–1277, 1962.
[2] O. Acher, P. Baclet, and G. Perin, "Investigation of the microwave permeability of ferromagnetic film laminations under a magnetic field," *J. Magn. Magn. Mater.*, vol. 157/158, pp. 480–481, 1996.
[3] V. V. Ustinov, A. B. Rinkevich, and L. N. Romashev, "Microwave magnetoresistance of Fe/Cr multilayers in current-perpendicular to plane geometry," *J. Magn. Magn. Mater.*, vol. 198/199, pp. 82–84, 1999.
[4] P. B. Johns and R. L. Beurle, "Numerical solution of two-dimensional scattering problems using a transmission-line matrix," *Proc. IEEE*, vol. 118, pp. 1203–1209, 1971.
[5] J. R. Rebel, M. Aidam, and P. Russer, "On the convergence of the classical symmetrical condensed node-TLM scheme," *IEEE Trans. Microwave Theory Tech.*, vol. 49, pp. 954–963, May 2001.
[6] P. B. Johns, "A symmetrical condensed node for the TLM method," *IEEE Trans. Microwave Theory Tech.*, vol. MTT-35, pp. 370–377, Apr. 1987.
[7] J. L. Herring, "Developments in the transmission-line modeling method for electromagnetic compatibility studies," Ph.D. dissertation, Unive. Nottingham, Nottingham, U.K., 1993.
[8] R. Ciocan, "Numerical models for elastic and electromagnetic wave propagation with applications to nondestructive characterization of materials," Ph.D. thesis, Univ. Akron, Akron, OH, 2003.
[9] H. Jin and R. Vahlidieeck, "Direct derivation of TLM symmetrical condensed node and hybrid symmetrical condensed node from Maxwell's equations using centered difference and averaging," *IEEE Trans. Microwave Theory Tech.*, vol. 42, pp. 2554–2561, Dec. 1994.
[10] K. S. Yee, "Numerical solution of initial boundary value problems involving Maxwell's equation in isotropic media," *IEEE Trans. Antennas Propagat.*, vol. 14, pp. 302–307, May 1966.
[11] M. Krumpholz, C. Huber, and P. Russer, "A field theoretical comparison of FDTD and TLM," *IEEE Trans. Microwave Theory Tech.*, vol. 43, pp. 1935–1950, Aug. 1995.
[12] P. B. Johns, "On the relation between TLM and finite difference methods for Maxwell's equations," *IEEE Trans. Microwave Theory Tech.*, vol. 35, pp. 60–61, Jan. 1987.
[13] R. Allen, A. Mallik, and P. Johns, "Numerical results for the symmetrical condensed TLM node," *IEEE Trans. Microwave Theory Tech.*, vol. 35, pp. 378–382, Apr. 1987.
[14] M. Celuch-Marcysiak and W. K. Gwarek, "Formal equivalence and efficiency comparison of the FD-TD, TLM and SN methods in application to microwave CAD programs," in *Proc. 21st Microwave Conf.*, vol. 1, Stuttgart, Germany, 1991, pp. 199–204.
[15] V. Trenkic, C. Christopoulos, and T. M. Benson, "Analytical expansion of the dispersion relation for TLM condensed nodes," *IEEE Trans. Microwave Theory Tech.*, vol. 44, pp. 2223–2230, Dec. 1996.
[16] A. Taflove, *Computational Electrodynamics: The Finite-Difference Time-Domain Method*.   Boston, MA: Artech House, 1995, pp. 23–35.
[17] V. Trenkic, C. Christopoulos, and T. M. Benson, "Simple and elegant formulation of scattering in TLM nodes," *Electron. Lett.*, vol. 29, pp. 1651–1652, 1993.
[18] D. M. Pozar, *Microwave and RF Wireless Systems*.   New York: Wiley, 2001, pp. 50–53.
[19] R. Ciocan, "Evanescent microwave microscope: A novel nondestructive, high resolution method for quantitative evaluation of materials," M.S. thesis, Case Western Reserve Univ., Cleveland, OH, 2000.
[20] N. Ida, *Microwave NDT*.   Amsterdam, The Netherlands: Kluwer, 1992, pp. 201–273.